Chapter 6

An *in vivo* toxicity assessment of piezoelectric $Na_xK_{1-x}NbO_3$ (x = 0.2 – 0.8) nanoparticulates towards bone tissue engineering approach

This chapter discusses about an in vivo study to examine the local and systemic toxicity of NKN nanoparticulates in rat's model, as a first report. As initial screening of toxicity, osteoblast-like MG-63 cells were exposed with different eluate concentrations (0.25, 2.5, 25 mg/ml) of $Na_xK_{1-x}NbO_3$ (x = 0.2 - 0.8). Thereafter, the potential biocompatibility of NKN nanoparticulates was investigated by intra-articular injection of the highest concentration (25 mg/ml) of prepared eluates in the knee joint of rats for 7 days. The histological analyses, as well as inflammatory cytokines profiling of these organs, were performed to observe any sign of inflammation. In addition, the biochemical assays (Alkaline phosphatase and Creatinine activities) of extracted blood serum of the particulate treated groups of rats were performed to grossly examine the functionality of organs.

6.1. Characterization of $Na_xK_{1-x}NbO_3$ nanoparticulates

XRD analyses of calcined (microsized) and planetary ball milled (nanosized) $Na_xK_{1-x}NbO_3$ (x = 0.2, 0.5, 0.8) powder are shown in Fig. 6.1. XRD patterns indicate the presence of a single phase monoclinic structure of NKN (JCPDS # 77-0038). The crystallite size (obtained from Scherrer's formula), decreased from (29 to 23 nm), (19 to 15) and (13 to 11 nm) for $Na_xK_{1-x}NbO_3$ x = 0.2, x = 0.5, x = 0.8, respectively, after 10 h of planetary ball milling. The crystallite size continuously decreases from x = 0.2 to 0.8, which may be due to decrease in potassium content having comparatively larger size (K ionic radii: 0.164 nm) than sodium (Na ionic radii: 0.164 nm). An enlarged view is revealing the shift in the position of the most

intense diffraction peak and decrease in peak intensity after planetary ball milling, attributed to the decrease in crystallite size and crystallinity, respectively.

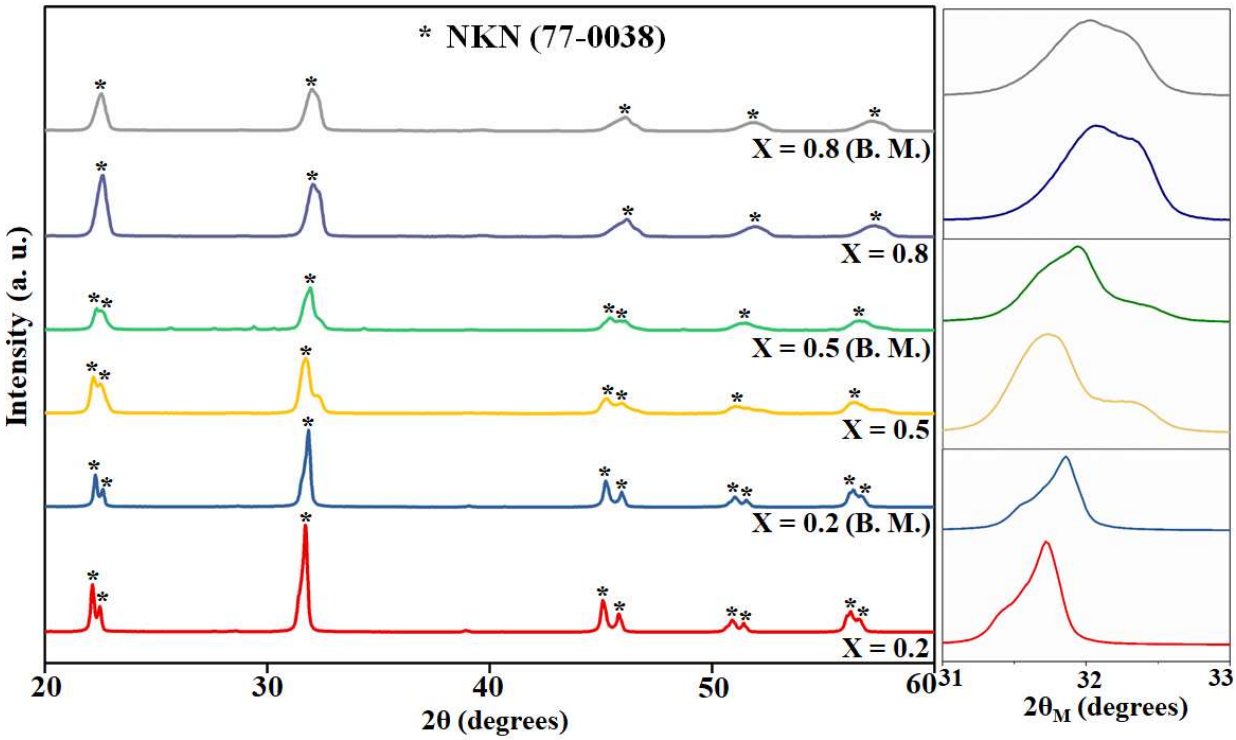

Fig. 6.1. X-ray diffration pattern of micro-sized and nano-sized (after 10 h planetary ball milling) $Na_xK_{1-x}NbO_3$ (x = 0.2 - 0.8) powders. Enlarged view illustrating the position and intensity of most intense diffraction peaks of NKN samples before and after ball milling. (B. M: Planetary ball milling).

6.2. Morphological analyses

The high resolution scanning electron microscopy (HRSEM) images and corresponding EDS graphs for $Na_xK_{1-x}NbO_3$ (x = 0.2 - 0.8) nano-powders are shown in Fig. 6.2. The average particle size of ball-milled $Na_xK_{1-x}NbO_3$ (x = 0.2, 0.5, 0.8) nano-powders varies as 70–180 nm, 80–170 nm and 70–160 nm, respectively with the almost polyhedral shapes. The particle size distribution of $Na_xK_{1-x}NbO_3$ (x = 0.2, 0.5, 0.8) powders in saline were measured in the

range of 600-1100 nm, 680-1200 nm and 650-1150 nm, respectively, which indicate the agglomeration of NKN particulates in the aqueous medium.

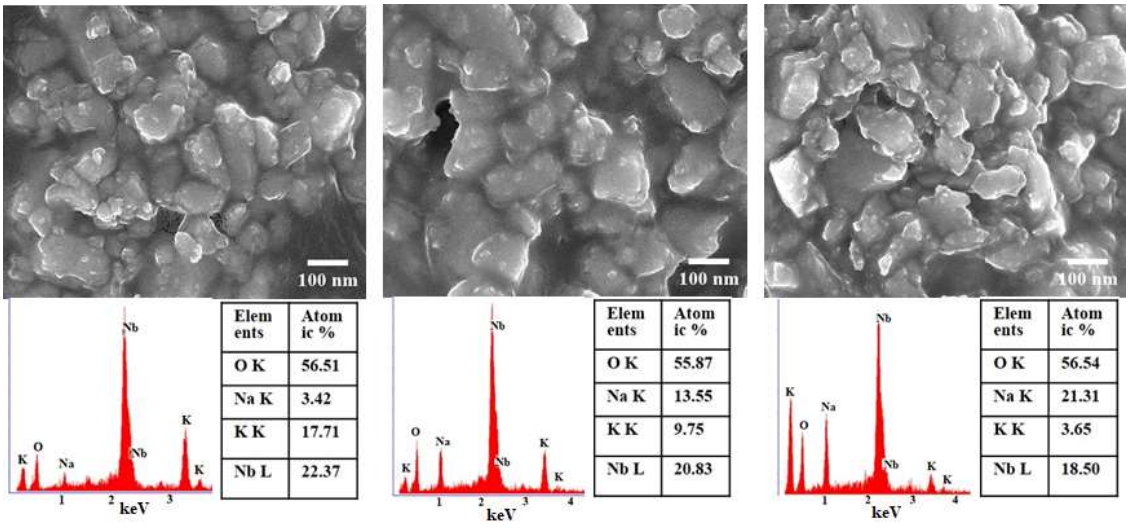

Fig. 6.2. High resolution scanning electron microscopy (HRSEM) images and EDS graphs for $Na_xK_{1-x}NbO_3$ nano-powders, (a) x = 0.2, (b) 0.5, (c) 0.8, planetary ball milled for 10 h.

6.3. Initial screening of toxicity (Cell culture study)

To investigate the viability of cells, different concentrations C1, C2, C3 of N1, N2, N3 nano-powders were exposed to the MG-63 cells. Fig. 6.3 demonstrates the morphology and viability of MG-63 cells on NKN nanoparticulates after 24 and 72 h of seeding. The cell morphologies are observed to be similar among control and different concentrations of three NKN samples [Fig. 6.3 (A)]. MTT results suggest that the initial viability (after 24 h) of cells in NKN treated samples is slightly lower than the control sample [Fig. 6.3 (B)]. In addition, the viability of cells is higher in eluates with lower concentration i.e., C1 (0.25 mg/ml) of NKN particulates than in higher concentrations (C2 and C3) i.e., the viability on the NKN samples decreases with the increase of concentration. It is probably due to the physical damage of cells with nanoparticles. After 72 h, the cell density and viability of cells are almost similar in all concentrations of NKN samples and the control group [Figs. 6.3 (A) and

(B)]. It is interesting to note that the sodium (i.e., $Na_{0.8}K_{0.2}NbO_3$) and potassium ($Na_{0.2}K_{0.8}NbO_3$) rich eluates reveal comparatively higher viability of cells than $Na_{0.5}K_{0.5}NbO_3$ eluates, after 72 h of culture. It may be due to the comparatively higher release of Na^+ and K^+ ions in the case of sodium and potassium rich compositions than $Na_{0.5}K_{0.5}NbO_3$. The release of Na^+ or K^+ ions causes a slight increase in the pH of culture media in a time dependent manner which may be the possible reason for the higher viability of cells [1, 2, 3]. Overall, the *in vitro* study reveals that the NKN nanoparticulates not only preserve the morphology of MG-63 cells but also facilitate their proliferation.

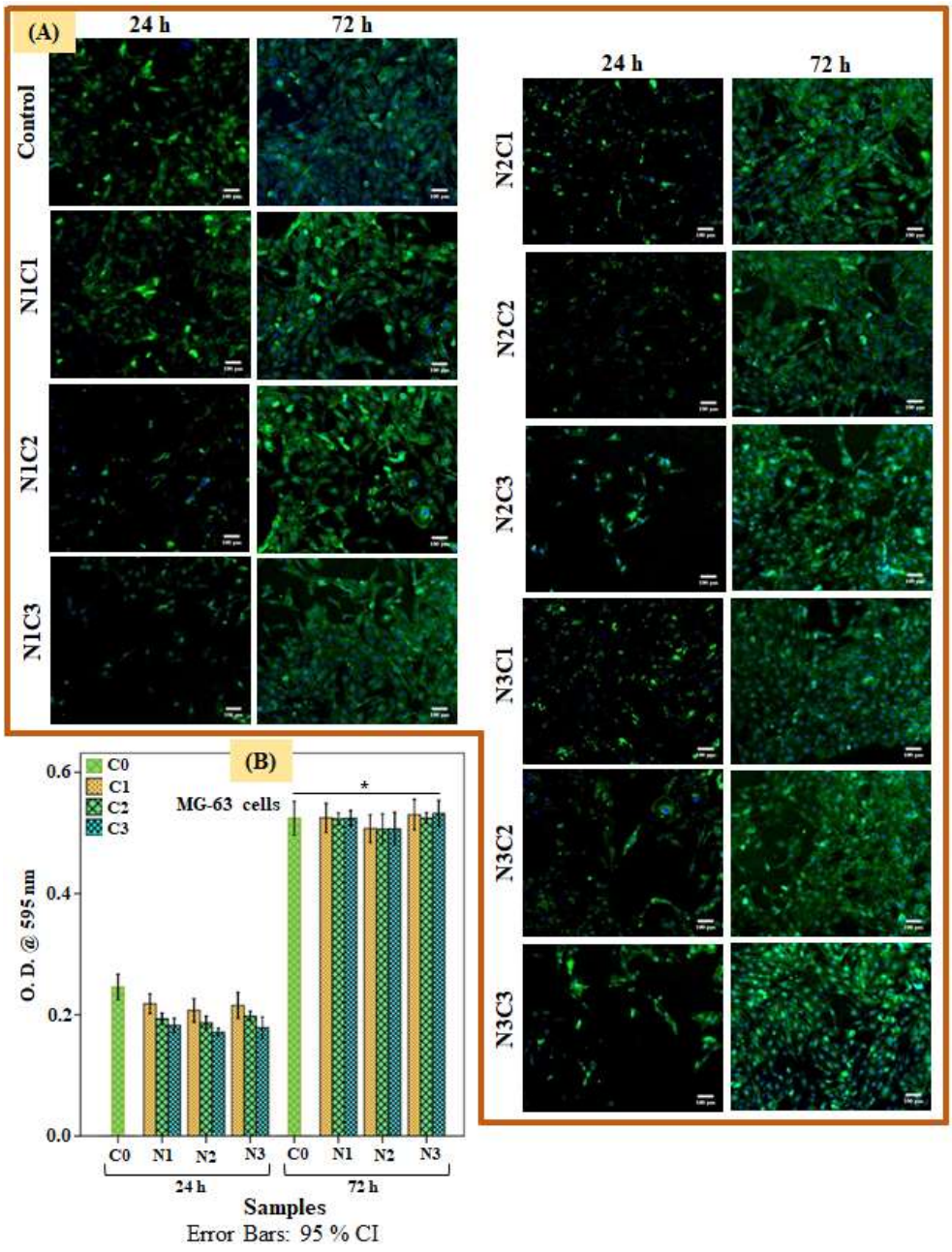

Fig. 6.3. (A) Qualitative and (B) quantitative response of MG-63 cells after 24 and 72 h of culture on $Na_xK_{1-x}NbO_3$ (x = 0.2, 0.5, 0.8) nanopowders i.e., N1, N2, N3 of concentrations, C1 (0.25 mg/ml), C2 (2.5 mg/ml) and C3 (25 mg/ml). Scale bar = 100 µm. Asterisk mark (*) represents the statistically significant difference in the mean optical density among all of the NKN samples (N1, N2 and N3) of different concentrations after 72 h of culture with respect to the mean optical density of the respective samples after 24 h of culture.

6.4. Animal study

6.4.1. General observations

During the 7 days of NKN particulate injection in the knee (synovial) joint of rats, no changes in skin texture and salivation in rats were observed. The rats did not suffer from diarrhea, tremor, or convulsion and were not in the comatose stage, post intra-articular injection. Further, there were no significant changes in the behavioral activities of all of the rats during 7 days of obsevation. The site of injections in all groups of rats was also free from any kind of inflammation (redness or swelling) in gross inspection during 7 days of treatment. The images of the paws of the particulate treated rats were captured using a digital camera, which was compared with the paws of control and saline treated groups of rats. The paws of the NKN nanoparticulates (N1, N2 and N3) injected rats were found to be similar to the saline and control rats without any sign of edema, redness, inflammation or any sign of deformities, as shown in Fig. 6.4. Similarly, the synovial joint in the treated, saline and control rats exhibited normal morphology at the end of the experimental protocol. Moreover, any inflammation at the injection site and atrophy of surrounding cartilage and bone tissues of the tibia and femur were absent. This finding corroborates well with the *in vitro* cytocompatibility results for NKN nanoparticulates of different compositions [Fig. 6.3 (B)].

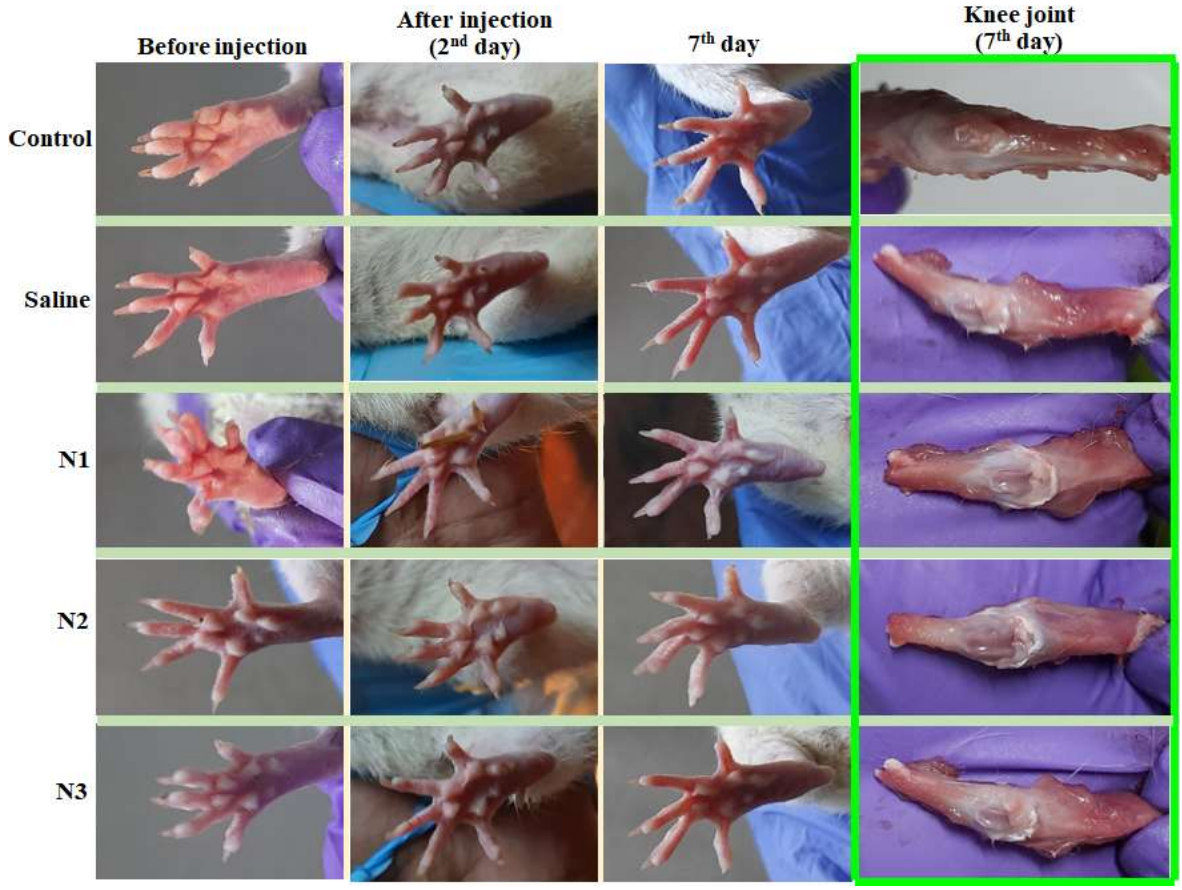

Fig. 6.4. Representation of the paws of the rats before and 7th days' post intra-articular injection of NKN nanoparticulates and the knee joint, confirming the absence of any inflammation.

6.4.2. Effect of intra-articular injection of N1, N2 and N3 compositions on the body weight

The change in body weight is an important parameter to access whether the injected nanoparticulates have caused any toxic effects on the functioning of vital organs [4, 5, 6]. Therefore, the weight of each of the 30 rats was measured before and after injection (up to 7 days). No significant variation in weight was recorded in the particulate injected, saline, and a control group of rats [Fig. 6.5].

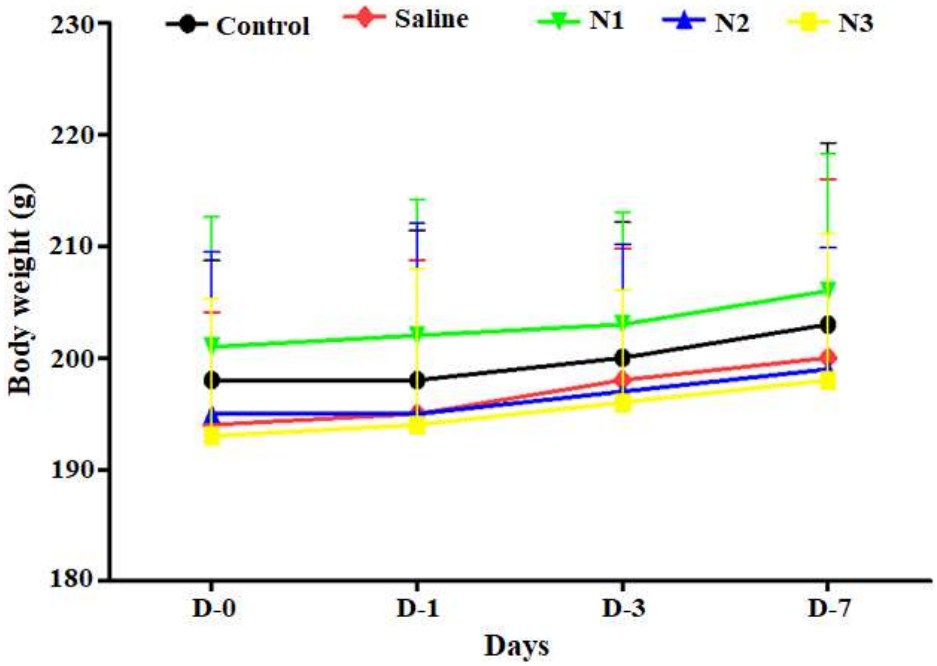

Fig. 6.5. Effect of intra-articular injection of N1, N2, and N3 compounds on body weight of the rats during the experimental protocol. All values are represented as mean ± SD (n = 6 rats/group) (Two-way ANOVA followed by Bonferroni post hoc test). Statistical analysis by two-way ANOVA revealed no significant changes in the body weight of the rats ($p > 0.05$).

6.4.3. Biochemical assay

Biochemical parameters of extracted serum were measured to evaluate the effects of NKN nanoparticulates induced changes in the serum level of enzymes of the treated rats. Generally, the level of serum ALP activity is measured to examine the hepatic function. The increase in ALP activity resembles the obstruction in liver functioning [7]. The death and healing of the liver tissue result in an increase and decrease in the hepatic ALP activity, respectively [8]. Furthermore, the chemical/drug induced hepatotoxicity or cholestasis also leads to the rise of ALP activity in blood serum [9, 10]. Therefore, the liver is an important organ to study the influence of particulate associated toxicity. Statistical analysis by one-way ANOVA shows no significant differences in the serum level of ALP among the NKN

particulate treated (N1, N2 and N3) and control groups [Fig. 6.6 (a)]. It can, therefore, be suggested that the functioning of the liver remains unaffected after exposure of NKN nanoparticles.

Moreover, the estimation of creatinine levels in serum is generally performed to analyze whether the biomaterials or "foreign particles" have any toxic effects on the functioning of the renal system [11]. The elevation of blood creatinine level indicates the obstruction in the filtering ability of the kidneys [12, 13, 14, 15]. In the present study, the level of creatinine in the blood serum of rats treated with N1, N2 and N3 nanoparticulates do not show any significant differences as compared to the control group [Fig. 6.6 (b)]. It indicates that NKN nanoparticulates have not caused kidney dysfunction.

The balanced concentration of sodium and potassium in the body plays an important role in regulating blood pressure and proper functioning of hepatic or renal systems [16, 17, 18, 19]. It has been demonstrated that inflammatory kidney disease reduces the activity of Na/K ATPase which consequently, results in the impairment of sodium and potassium in the intracellular/extracellular region of the renal system [20, 21]. In the present study, the sodium and potassium in all three NKN particulate treated rats did not cause any liver or kidney dysfunction. The release of sodium or potassium ions from injected NKN nanoparticulates may help in maintaining the proper balance of sodium and potassium in the cellular microenvironment which results in the absence of inflammation in the biochemical investigation. Overall, these findings suggest that the intra-articular injection of all of the NKN nanoparticulates in rats does not cause any kind of hepatic or renal disorder.

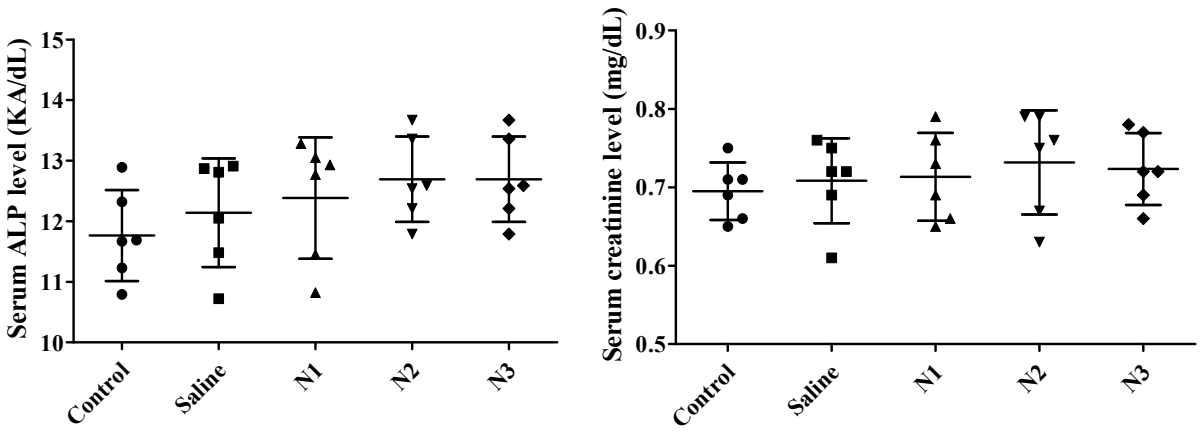

(a) *(b)*

Fig. 6.6. Effect of intra-articular injection of N1, N2, and N3 compounds on serum concentration of (a) Alkaline phosphatase activity (ALP) and (b) Creatinine, at the end of day 7 of the experimental protocol. All values are in mean ± SD (n=6 rats/ group). (One-way ANOVA followed by Newman-keuls multiple comparison post hoc test). Statistical analysis by one-way ANOVA revealed no significant changes in the serum ALP level and creatinine among the groups [$F_{(4,29)} = 1.386$; $p>0.05$].

6.4.4. Inflammatory cytokines analyses

The results, obtained from qRT-PCR for the liver and spleen are represented in Fig 6.7 (a) and (b), respectively. The qRT-PCR values for the liver indicated a small elevation in the expression of pro-inflammatory cytokines (TNF-α and IL-12) in the N1 (1.1 and 1.09 folds), N2 (1.15 and 1.13 folds), N3 (1.11 and 1.12 folds) and saline treated (1.19 and 1.18 folds) rats as compared to control rats [Fig. 6.7 (a)]. A similar trend was observed for the spleen, where the expression of pro-inflammatory cytokines (TNF-α and IL-12) are (1.08 and 1.09 folds), (1.14 and 1.12 folds), (1.06 and 1.08 folds) and (1.17 and 1.15 folds) for N1, N2, N3 and saline treated rats, respectively [Fig. 6.7 (b)]. It is also noticeable that the expression of proinflammatory cytokines of liver and spleen tissues for all of the NKN treated samples are

comparatively lower than the saline treated samples. Besides, the expression of proinflammatory cytokines for all three NKN particulates treated organs do not show any statistically significant difference with respect to saline treated or control samples. Apart from proinflammatory cytokines, qRT-PCR data elucidated that the expression of anti-inflammatory cytokines (IL-4 and IL-10) for liver tissue, increases in the N1 (1.39 and 1.41 folds), N2 (1.31 and 1.35 folds), and N3 (1.44 and 1.42 folds) treated samples with respect to control [Fig. 6.7 (a)]. For spleen tissues, the expression of anti-inflammatory cytokines (IL-4 and IL-10) increased by (1.43 and 1.39 folds), (1.29 and 1.31 folds) and (1.43 and 1.41 folds) with respect to control for N1, N2 and N3 samples, respectively [Fig. 6.7 (b)]. However, the expression of anti-inflammatory cytokines decreases (but not significantly) with respect to control on the saline treated tissues of rats for both of the organs i.e., (IL-4 and IL-10) for spleen and liver are (0.94, 0.96 fold) and (0.92, 0.94 fold), respectively. Although, all of the N1, N2 and N3 treated samples are showing a statistically significant increase in the expression of anti-inflammatory cytokines with respect to saline treated samples of rats [represented as '#' in Fig 6.7 (a) and (b)], the potassium and sodium rich NKN i.e., $Na_{0.2}K_{0.8}NbO_3$ (N1) and $Na_{0.8}K_{0.2}NbO_3$ (N3) treated rats are showing significantly higher expression of anti-inflammatory cytokines (IL-4 and IL-10) with respect to control for both of the inspected organs [represented as '*' in Fig 6.7 (a) and (b)]. It has been demonstrated that inflammatory conditions (caused by infection or allergy) alter the transportation of ions such as sodium, potassium, chloride etc. [21]. Overall, these findings clearly suggest that the NKN nanoparticulates are not only easily adaptable by the host tissues but also strengthen the inflammation alleviating response.

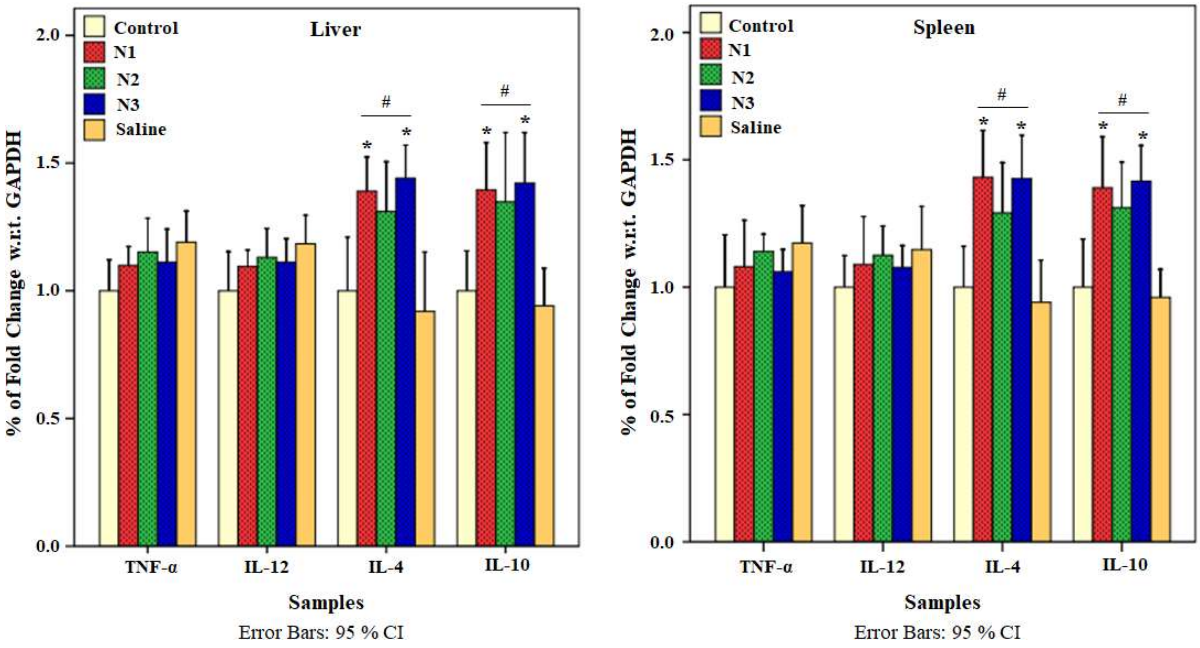

Fig. 6.7. The plots representing the percentage of fold change (w. r. t. GAPDH) in gene expression of proinflammatory (TNF-α and IL-12) and anti-inflammatory (IL-4 and IL-10) cytokines for N1, N2, N3 treated, saline treated and control (non-injected) rats in (a) liver and (b) spleen. Asterisk marks "" and "#" represent the statistically significant difference in the mean values of gene expression of NKN treated samples with respect to control and saline treated samples, respectively, at $p \leq 0.05$ (n = 6 rats/ group).*

6.4.5. Histopathological analyses (hematoxylin and eosin staining)

The histological analyses were performed to evaluate the particulate toxicity induced changes in the microarchitecture of the vital organs such as heart, liver, kidney and spleen of rats after intra-articular injection of N1, N2 and N3 nanoparticles. The histological images of the hematoxylin and eosin stained organs of particulate (N1, N2 and N3) treated groups were represented with the control and saline treated groups for comparison [Fig. 6.8, 6.9, 6.10 and 6.11].

The histological images of heart tissues of all of the NKN treated (N1, N2 and N3) groups do not show any sign of cardiac muscle disarray, vacuolization, hemorrhage or tissue shrinkage and their muscle fibers were found to be straight and organized as well, similar to the control groups [Fig. 6.8]. Connective tissues of hearts demonstrate normal architecture in the particulate treated groups of rats. It has been reported that exposure of fine concentrated particles leads to abnormal heart rate and sometimes causes cardiac dysfunction [22, 23, 24, 25, 26]. In a previous study, swelling in endothelial cells of the heart was observed after the injection of TiO_2 nanoparticulates for 7 days [27]. However, no swollen endothelial cells were observed in the hearts of N1, N2 and N3 eluates treated groups of rats [Fig. 6.8]. Overall, no histological changes were found in the hearts tissues of NKN (N1, N2 and N3) treated rats.

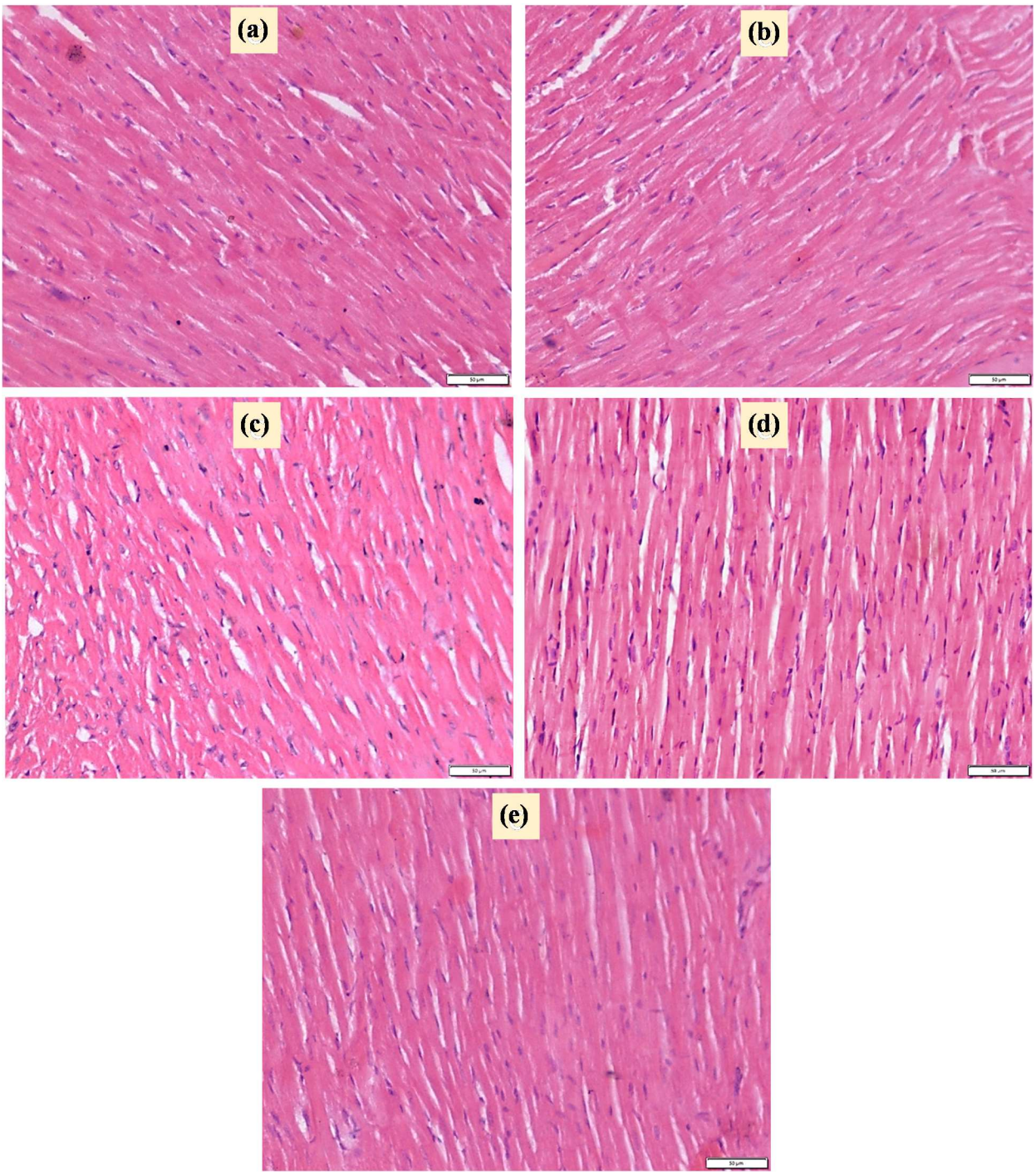

Fig. 6.8. Histopathological images of hematoxylin and eosin (H & E) stained heart tissues of (a) Control (non-injected), (b) Saline, (c) N1, (d) N2 and (e) N3 nanoparticulate eluates treated groups of rats after 7 days of intra-articular injection. The muscle fibers are well

organized and connective tissues of hearts demonstrate normal architecture in the particulate treated and control groups of rats.

The liver is an important organ that participates in the detoxification process. Therefore, there may be the possibility that the foreign particles translocate to the liver through the lymphatic or circulatory system [28, 29, 30]. Cytoplasmic vacuolization leads to the interruption in membrane functionality and sometimes indicates injury in the liver [31, 32, 33]. In our study, no cytoplasmic vacuolization of hepatocytes was found in the livers of NKN treated groups of rats. The sizes of nuclei of hepatocytes and endothelial cells also appear to be similar in the particulate treated, saline and control rats. In addition, there is no indication of translocation of NKN nanoparticulates in the liver. Overall, histological images of livers of rats, treated with NKN particulates (N1, N2 or N3), did not show any sign of necrosis, injury, hemorrhage around the sinusoids or central venules, which rather observed to be normal and similar to the saline and control rats [Fig. 6.9]. These findings corroborate the biochemical marker (ALP) to check the functionality of the liver, where no significant elevation was observed in the particulate treated and control rats [Fig. 6.6 (a)]. Overall, the histological examination indicates the absence of any toxicity in the NKN particulate treated livers which also confirms the results obtained from the inflammatory cytokines (TNF-α and IL-12) profile analyses [Fig 6.7 (a)].

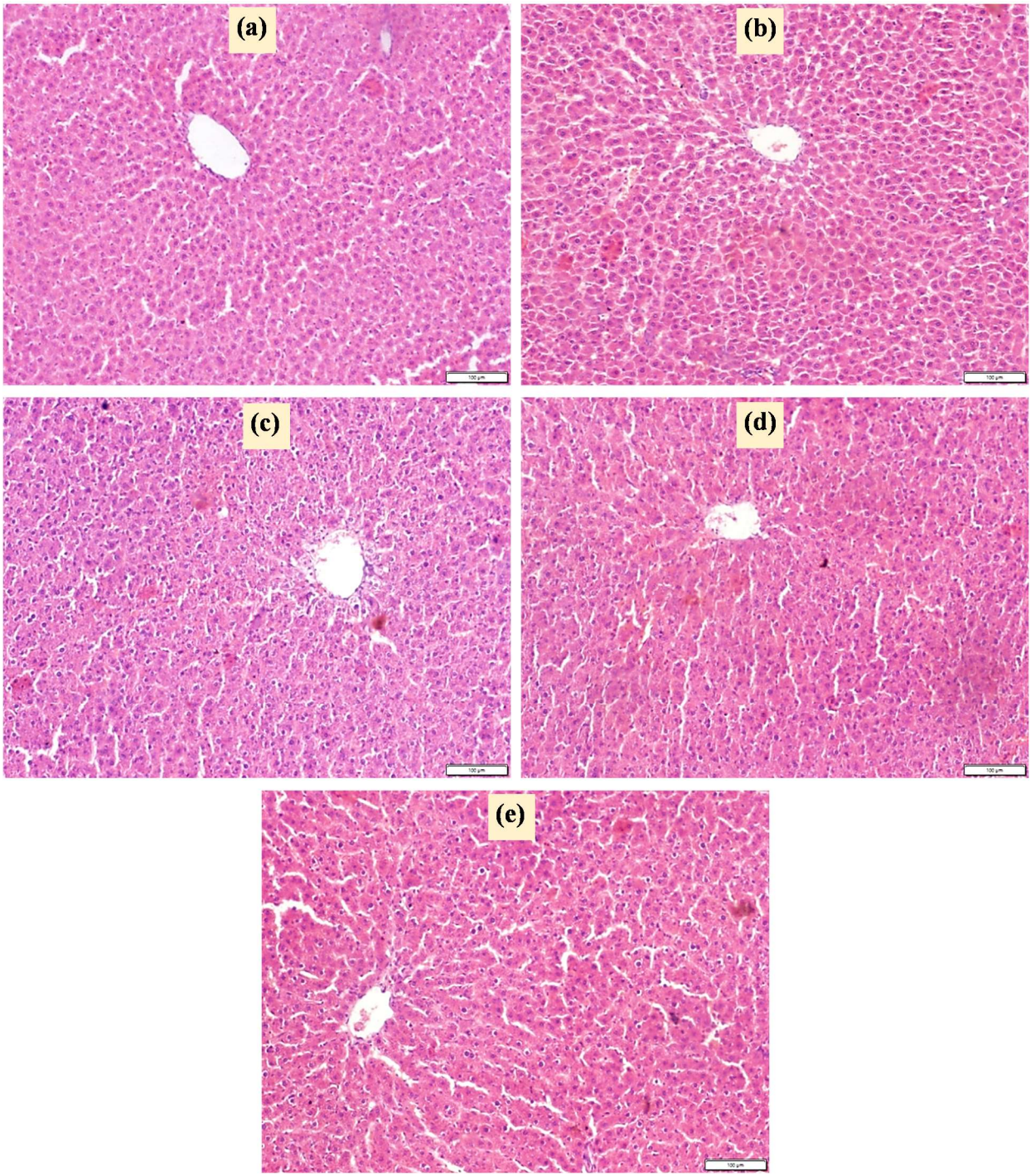

Fig. 6.9. Histopathological images of H & E stained liver tissues of (a) Control (non-injected), (b) Saline, (c) N1, (d) N2 and (e) N3 nanoparticulate eluates treated groups of rats after 7 days of intra-articular injection. The sizes of nuclei of hepatocytes and endothelial cells appear to be similar in the particulate treated, saline and control rats.

The kidney plays an important role in the clearance of metabolites or waste products by filtering out the xenobiotics from the body and therefore, the kidney must participate in the discharge of nanoparticulates, if reached to the vital organs. In this perspective, the histological examination of kidney tissue is important not only to trace the nanoparticulates but also to investigate the influence of nanoparticulates on the functioning and architecture of the kidneys. Several studies suggested that the exposure of nanoparticulates (Au, ZnO, TiO_2) results in pathological changes in the kidney such as tubules dilation, scattered glomeruli, necrosis, etc. [27, 34, 35, 36]. However, the histological images of the kidney section of NKN particulate (N1, N2 and N3) treated rats are revealing normal nephric tubules (without any sign of vacuolar degeneration) within the cortex, similar to control rats [Fig. 6.10]. In addition, the histological images of the kidney section of NKN treated and control rats demonstrate normal glomerular tufts and renal cortex without tubules dilation or necrosis. Inclusively, the histological analyses of the kidney section revealed that the intra-articular injection of NKN nanoparticulates (N1, N2 and N3) does not produce any toxic effect on the renal system. These findings further substantiate the creatinine level, measured using serum extracted from particulate treated rats [Fig. 6.6 (b)].

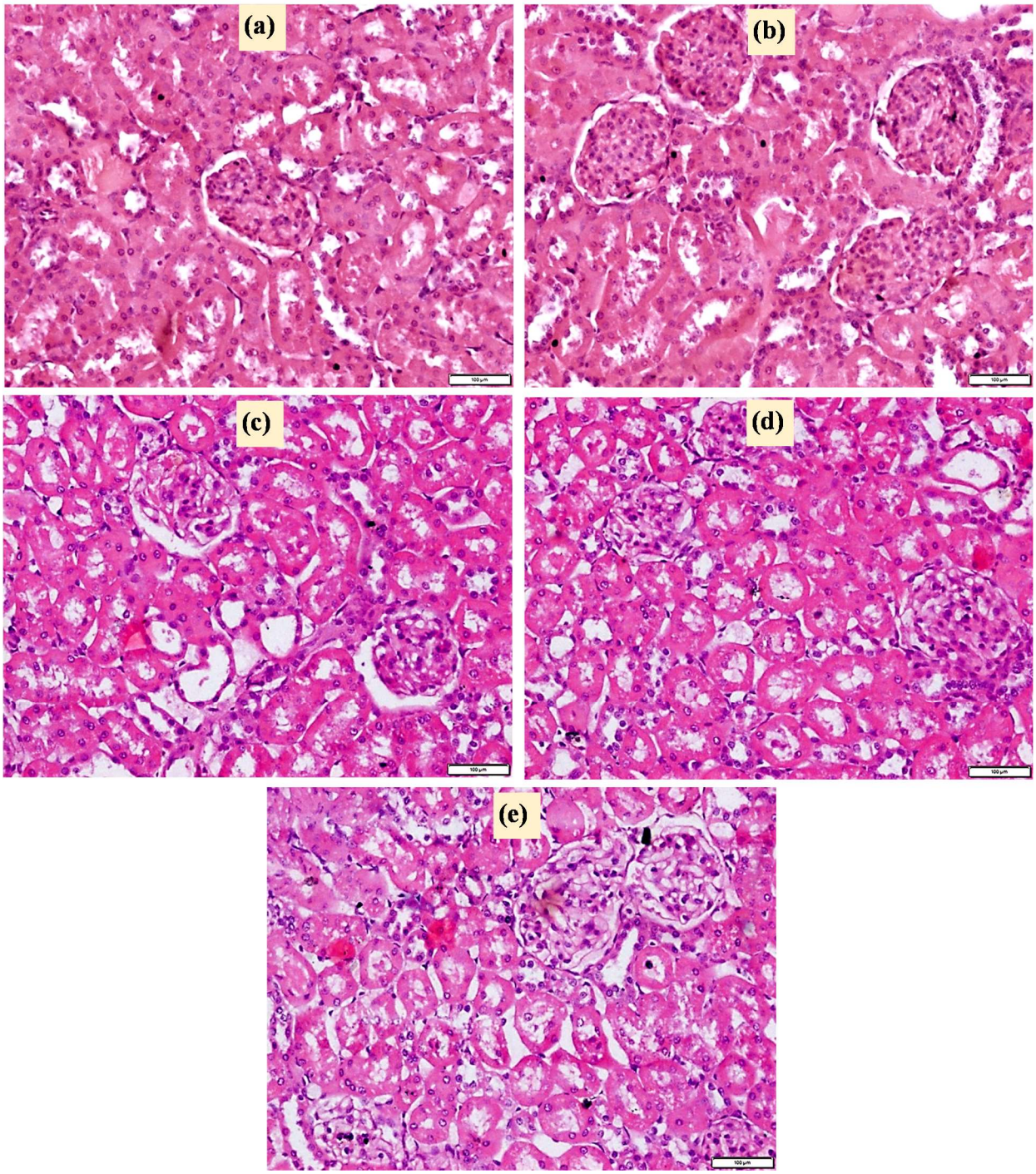

Fig. 6.10. Histopathological images of H & E stained kidney tissues of (a) Control (non-injected), (b) Saline, (c) N1, (d) N2 and (e) N3 nanoparticulate eluates treated groups of rats after 7 days of intra-articular injection. The particulate treated rats are revealing normal nephric tubules within the cortex, similar to control rats. In addition, the particulate treated

and control rats demonstrate normal glomerular tufts and renal cortex without tubules dilation or necrosis.

Apart from liver, the spleen is another leading target organ having the possibility for the accumulation of foreign nanoparticulates through systematic circulation [28, 37, 38, 39, 40]. The histological examination of the spleen section of NKN (N1, N2 and N3) nanoparticulates treated rats demonstrates the normal architecture of splenic pulp, lymphoid follicles, white pulp, red pulp (including blood sinusoids) and fibrous trabecular, similar to control rats [Fig. 6.11]. In addition, there was no visual sign of cellular damage or any trace of particles dissemination. The histological assessments of the NKN particulate treated spleens do not reveal any sign of toxicity and these findings are in agreement with the proinflammatory cytokines (TNF-α and IL-12) profile examination which also indicates the absence of inflammation in the NKN treated spleen tissues [Fig. 6.7 (b)].

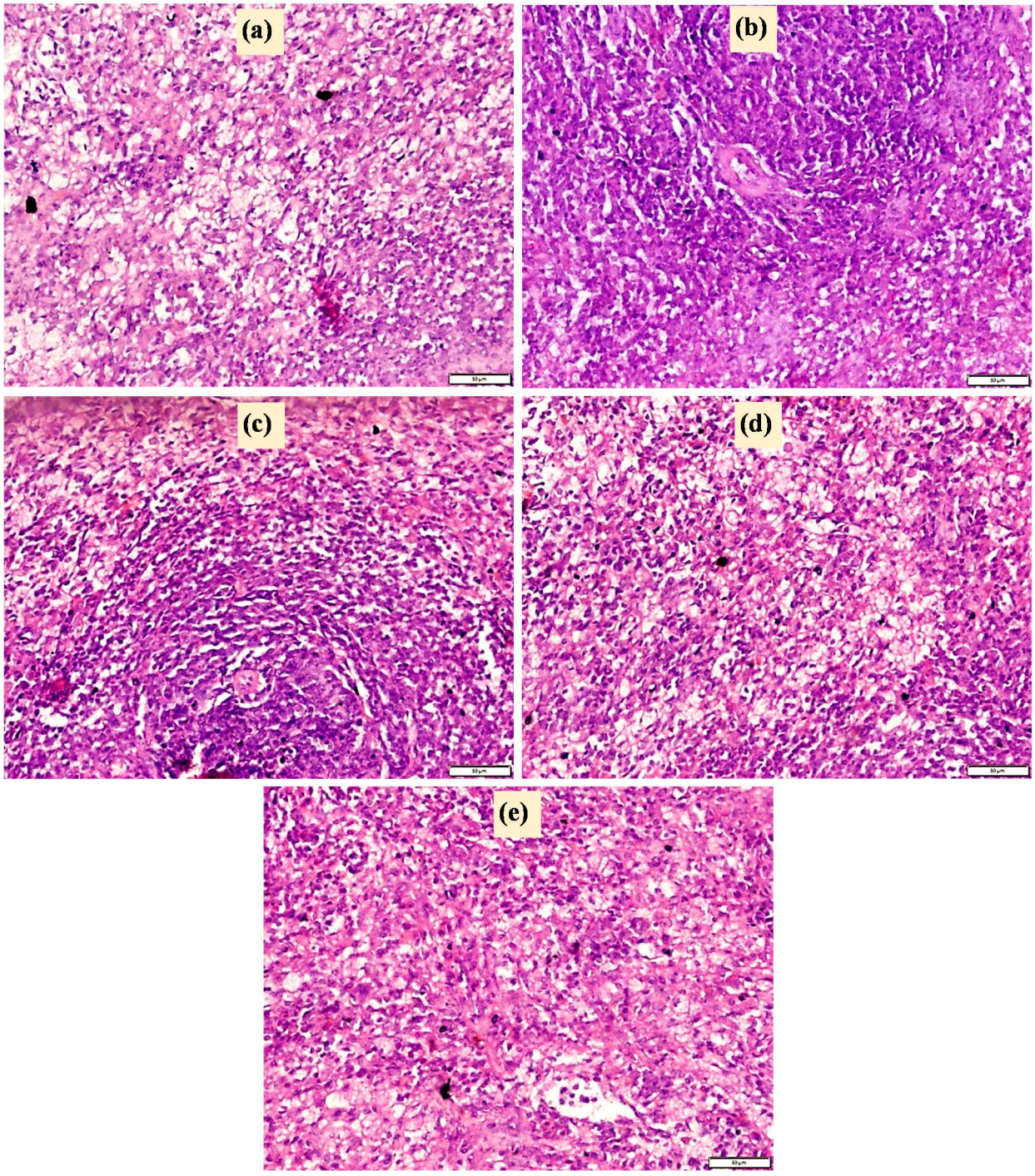

Fig. 6.11. Histopathological images of H & E stained spleen tissues of (a) Control (non-injected), (b) Saline, (c) N1, (d) N2 and (e) N3 nanoparticulate eluates treated groups of rats after 7 days of intra-articular injection. The NKN (N1, N2 and N3) nanoparticulates treated

rats demonstrate the normal architecture of splenic pulp, lymphoid follicles, white pulp, blood sinusoids and fibrous trabecular, similar to control rats.

Overall, it has been observed that the histological images of hematoxylin and eosin stained organs of N1, N2 and N3 nanoparticulates injected groups appeared normal and of similar structure as that of control and saline treated groups. Additionally, no sign of particles dissemination is observed in the vital organs of the particulate treated groups of rats.

In the histological section of the synovial joint of the treated rats, the accumulation of nanoparticulates can be observed between the bones around the cartilage, as depicted in Fig 6.12. Further, as can be seen in Figs. 6.12 (c), (d) and (e), there is no infiltration of macrophages which confirms the biocompatibility of the developed NKN nanoparticles. The infiltration increases with foreign particles as it is the second line of defense [41, 42]. Besides, the intra-articulate injection of the NKN nanoparticulates did not cause any damage to the articulate cartilage without any sign of synovial hyperplasia. Synovial hyperplasia is the clinical condition that is caused due to increase in cellularity of the synovial membrane due to the influx of different cellular components resulting in the thickening of the synovial membrane [43, 44, 45]. Moreover, this pathological condition also occurred due to excessive infiltration of immunoreactive cells [43, 46, 47]. Therefore, it can be affirmed that the intra-articulate injection of NKN nanoparticulates did not cause any histological changes in the bones and cartilage.

The histological analyses of the heart, liver, kidney, spleen and knee demonstrate normal architecture without any trace of NKN nanoparticulates. These findings are in agreement with the results, obtained from biochemical assays and inflammatory cytokines profiling (TNF-α and IL-12) [Fig. 6.6 and 6.7].

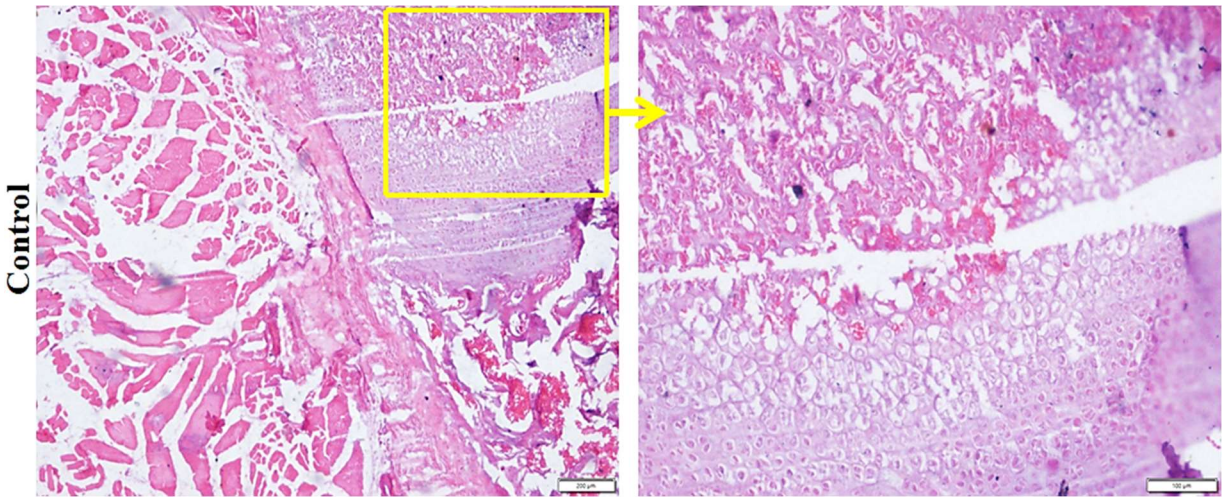

(a)

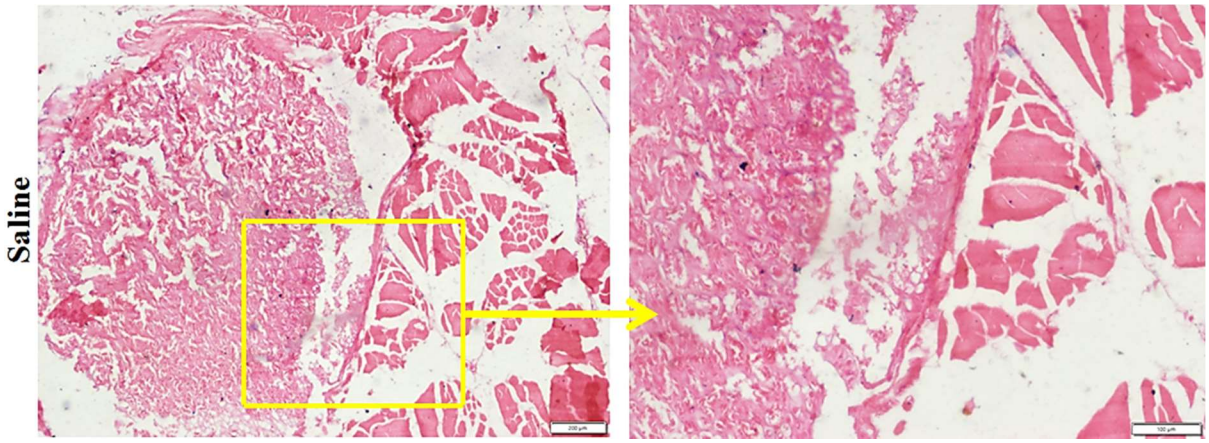

(b)

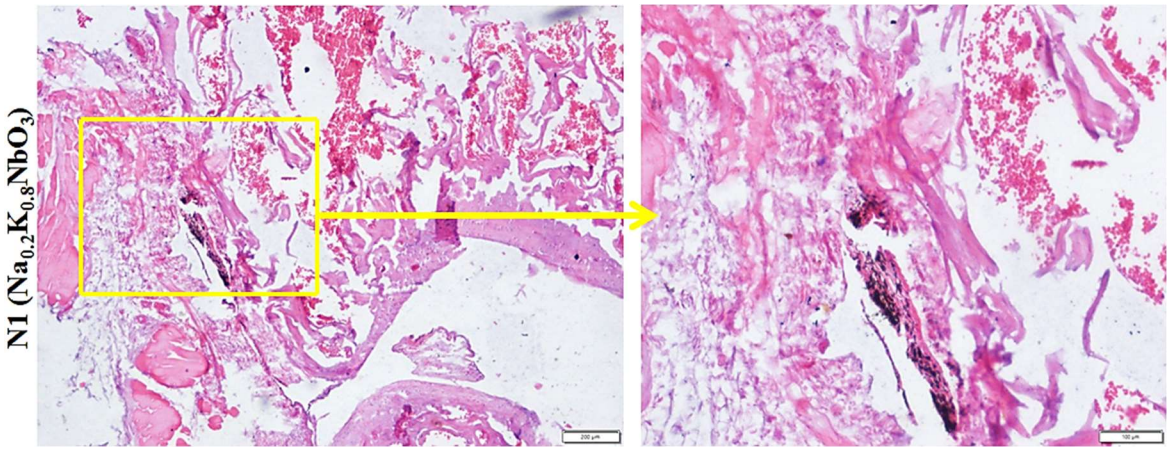

(c)

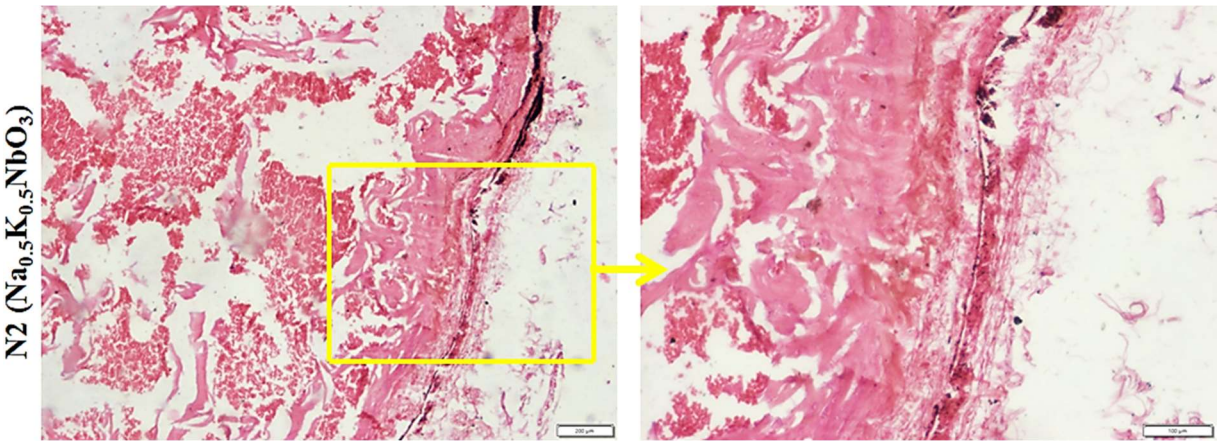

(d)

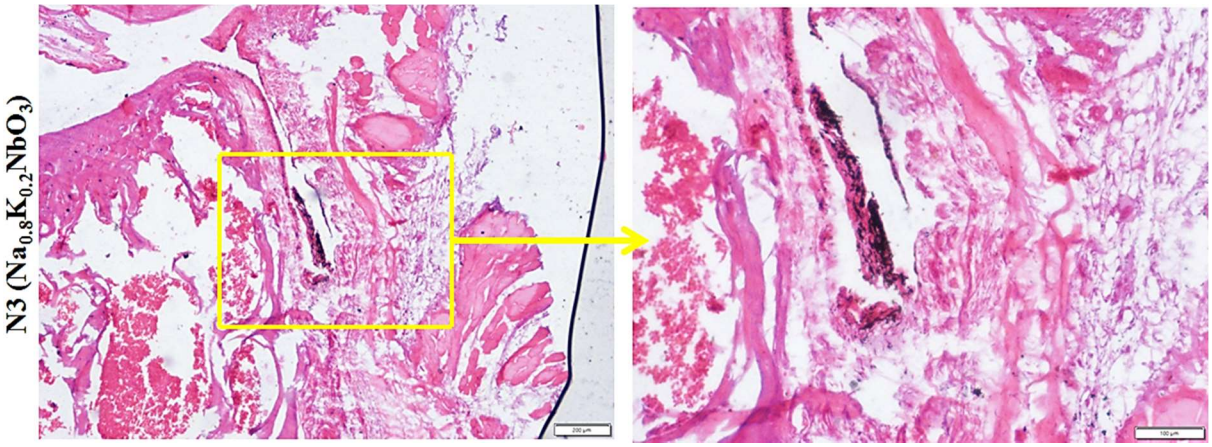

(e)

Fig. 6.12. Histopathological images of H & E stained knee joint tissues of (a) Control (non-injected), (b) Saline, (c) N1, (d) N2 and (e) N3 nanoparticulate eluates treated groups of rats after 7 days of intra-articular injection. NKN treated knee joint tissues are showing smooth cartilage (without any damage) with the deposition of particles.

Wear debris particles can cause unfavorable biological responses at the sites of implantation leading to prosthetic osteolysis and aseptic loosening [48, 49, 50, 51]. Wear debris particles induced inflammation promotes the recruitment of inflammatory cells as well as osteoclasts [48, 52, 53]. It ultimately creates an imbalance between the production of bone forming and

resorbing cells, which results in osteolysis [48, 54]. Such problems sometimes result in revision surgery in such patients. However, the histological analyses of NKN (N1, N2 and N3) nanoparticulates treated rats demonstrate no sign of inflammation at the injected site (knee joint) and vital organs [Figs. 6.8 to 6.12]. In addition, NKN nanoparticulates facilitate the growth of osteoblast-like MG-63 cells and did not cause any cytoskeletal disruption [Fig. 6.3]. Overall, NKN nanoparticulates are found to be cytocompatible (*in vitro*) and biocompatible (*in vivo*). The sodium and potassium ions create a favorable microenvironment in the extracellular matrix, renal and hepatic systems and these ions help in regulating the functionality of such organs (Sections 6.3, 6.4.3 and 6.4.4). Apart from sodium and potassium, niobium has also been suggested to be cytocompatible [55, 56, 57, 58]. Several researchers demonstrated the potentiality of niobium incorporated ceramics, polymer, bioglass and metal-based biomaterials for biomedical applications such as niobium doped 45S5 bioactive glass, β-titanium alloy, etc. [55, 59, 60, 61, 62, 63, 64, 65]. In contrast, the above discussion anticipates the non-toxic nature of sodium, potassium and niobium ions and therefore, corroborates the findings obtained in the present study which indicates the biocompatible nature of NKN nanoparticulates, injected in the knee joint of rats.

The adverse biological response of implanted wear debris particles such as aseptic loosening, osteolysis or inflammation depends upon the size, volume and morphology (shape) of wear particles [66, 67, 68, 69, 70]. Generally, the size of wear debris particles for ceramic-based implants such as ZrO_2 and Al_2O_3 are found to be in submicron range [71, 72]. Previous studies reported the engulfing of submicron-sized particles by the macrophages that increase the possibility of adverse reaction or inflammation [66, 70, 73]. However, no sign of macrophages infiltration was observed in the histological analyses of NKN particulate treated

knee joints (Fig. 6.12 (c), (d) and (e)), which indicates the biocompatibility of NKN nanoparticles.

It has been suggested that the nano-sized wear debris particles can translocate to the distal organs via the circulatory system and have the potential risk of dissemination across the body [27, 71, 72, 74]. However, the histological analyses did not indicate any translocation of NKN nanoparticulates in vital organs, after 7 days of intra-articular injection. The high-resolution microscopy and dynamic light scattering study reveal that the size of NKN (N1, N2 and N3) nanoparticulates are found in the range of 70 – 180 nm. However, size of the agglomerates are about 600 – 1300 nm. The agglomeration of NKN nanoparticulates in an aqueous solution may be the foremost cause of the absence of any trace of nanoparticulates in vital organs.

It can, therefore, be affirmed that NKN nanoparticulates are non-toxic and did not cause any inflammation. Overall, this study demonstrates the potentiality of NKN for bone tissue engineering applications.

Preliminary screening demonstrates that $Na_xK_{1-x}NbO_3$ (x = 0.2, 0.5, 0.8) eluates of different concentrations of upto 25 mg/ml, facilitate the attachment and proliferation of MG-63 cells. The histological investigation of the vital organs and knee of particulate eluates (25 mg/ml) treated rats did not reveal any morphological changes in the architecture of tissues, which confirms the non-toxic behavior of NKN nanoparticulates. The absence of any trace of nanoparticulates in the vital organs indicates that these nanoparticulates were not translocated to any of the vital organs. There was no sign of inflammation in the H and E stained images of knee tissues of particulate treated groups of rats. The inflammatory cytokines analyses of spleen and liver tissues of particulate treated groups of rats revealed the anti-inflammatory

potential of $Na_xK_{1-x}NbO_3$ (x = 0.2, 0.5, 0.8), which was comparatively higher for the sodium and potassium rich compositions of NKN than $Na_{0.5}K_{0.5}NbO_3$. Biochemical assays (ALP and Creatinine) of blood serum, extracted from the NKN particulates treated rats, revealed the normal functionality of liver and kidney, which further corroborated the results obtained from histopathological and inflammatory cytokines analyses. This study conclusively suggests the non-toxic behavior of NKN nanoparticulate sand thereby, takes NKN towards the next phase in the development of piezoelectric NKN-based bone mimicking implant.

References

[1] M. Uo M, M. Mizuno, Y. Kuboki, A. Makishima, F. Watari, Properties and cytotoxicity of water soluble Na_2O–CaO–P_2O_5 glasses, Biomaterials 19 (1998) 2277-2284.

[2] T. Arnett, Extracellular pH regulates bone cell function, J. Nutr. 138 (2008) 415S-418S.

[3] A. Galow, A. Rebl, D. Koczan, S. Bonk, W. Baumann, J. Gimsa, Increased osteoblast viability at alkaline pH *in vitro* provides a new perspective on bone regeneration, Biochem. Biophy. Rep. 10 (2017) 17-25.

[4] R. Lewis, R. Billington, E. Debryune, A. Gamer, B. Lang, F. Carpanini, Recognition of adverse and nonadverse effects in toxicity studies, Toxicol. Pathol. 30 (2002) 66–74.

[5] J. Hilaly, H. Israili, B. Lyoussi, Acute and chronic toxicological studies of *Ajuga iva* in experimental animals, J. Ethnopharmacol. 91 (2004) 43–50.

[6] S. Bailey, R. Zidell, R. Perry, Relationships between organ weight and body/brain weight in the rat: what is the best analytical endpoint? Toxicol. Pathol. 32 (2004) 448–466.

[7] M. Kaplan, A. Righetti, Induction of rat liver alkaline phosphatase: the mechanism of the serum elevation in bile duct obstruction, J. Clin. Invest. 49 (1970) 508-516.

[8] Z. Gawlik, E. Fiejka, R. Aleksandrowicz, I. Wiśniewska, Activity of alkaline phosphatase in the healing rat liver after hepatectomy, Folia Histochem Cytochem (Krakow) 16 (1978) 343-349.

[9] T. Wright, A. Vandenberg, Risperidone- and quentiapine-induced cholestasis, Ann. Pharmacother. 41 (2007) 1518-1523.

[10] A. Singh, T. Bhatm, O. Sharma, Clinical biochemistry and hepatotoxicity, J. Clin. Toxicol. , S4 (2011) 001.

[11] N. Panda, Kidney In: Textbook of Biochemistry and Human Biology. 2nd ed. Prentise Hall, India. (1999) 290-296.

[12] P. Chan P, O. Hara, W. Hayes, Principles and methods for acute and subchronic toxicity. In: principles and methods of toxicology. Hayes W.A. (ed). Raven Press N. Y. (1984) 351-376.

[13] O. Adeyemi, A. Elujoba, W. Odesanmi, Evaluation of the toxicity potential of Cassia podocarpa with reference to official senna. W. Africa, J. Pharmacol. D. Res. 8 (1988) 41-47.

[14] R. Oh, T. Hustead, Causes and evaluation of mildly elevated liver transaminase levels, American Family Physician 84 (2011) 1003–1008.

[15] A. Ene-ojo, E. Chinedu, F. Yakasai, Toxic Effects of Sub-Chronic Administration of Chloroform Extract of Artemisia maciverae Linn on the Kidney of Swiss Albino Rats, Int. J. Biochem. Res. Rev. 3 (2013) 119-128.

[16] Y. Choi, J. Lee, Y. Chang, M. Kim, E. Sung, H. Shin, S. Ryu, Dietary sodium and potassium intake in relation to non-alcoholic fatty liver disease, British J. Nutr. 116 (2016) 1447-1456.

[17] A. Mikkelsen, K. Thomsen, H. Vilstrup, L. Aamann, H. Jones, R. Mookerjee, S. Dutoit, J. Frystyk, N. Aagaard, Potassium deficiency decreases the capacity for urea synthesis and markedly increases ammonia in rats, Am. J. Physi-Gastr. Liver Physi. 320 (2021) G474-G483.

[18] S. Sharma, K. McFann, M. Chonchol, I. Boer, J. Kendrick, Association between Dietary Sodium and Potassium Intake with Chronic Kidney Disease in US Adults: A Cross-Sectional Study, Am. J. Nephrol. 37 (2013) 526-533.

[19] H. Koo, S. Hwang, T. Kim, S. Kang, K. Oh, C. Ahn, Y. Kim, The ratio of urinary sodium and potassium and chronic kidney disease progression, Medicine 97 (2018) e12820.

[20] U. Kuhnle, G. Guariso, M. Sonega, G. Hinkel, W. Hubl, D. Armanini, Transient pseudohypoaldosteronism in obstructive renal disease with transient reduction of lymphocytic aldosterone receptors, Horm. Res. 39 (1993) 152-155.

[21] M. Eisenhut, Changes in ion transport in inflammatory disease, J. Inflamm. 3 (2006).

[22] K. Timonen, E. Vanninen, J. Hartog, A. Mulli, B. Brunekreef, D. Gold, J. Heinrich, G. Hoek, T. Lanki, A. Peters, T. Tarkiainen, P. Tiittanen, W. Kreyling, J. Pekkanen, Effects of ultrafine and fine particulate and gaseous air pollution on cardiac autonomic control in subjects with coronary artery disease: the ULTRA study, J. Expo. Sci. Env. Epidemiol. 16 (2006) 332–341.

[23] D. Rich, W. Zareba, W. Beckett, P. Hopke, D. Oakes, M. Frampton, J. Bisognano, D. Chalupa, J. Bausch, K. O'Shea, Y. Wang, M. Utell, Are ambient ultrafine, accumulation mode, and fine particles associated with adverse cardiac responses in patients undergoing cardiac rehabilitation? Environ. Health Perspect. 120 (2012) 1162–1169.

[24] A. Peters, R. Hampel, J. Cyrys, S. Breitner, U. Geruschkat, U. Kraus, W. Jareba, A. Schneider, Elevated particle number concentrations induce immediate changes in heart rate variability: a panel study in individuals with impaired glucose metabolism or diabetes, Part. Fibre Toxicol. 12 (2015).

[25] R. Brook, J. Brook, B. Urch, R. Vincent, S. Rajagopalan, F. Silverman, Inhalation of fine particulate air pollution and ozone causes acute arterial vasoconstriction in healthy adults, Circulation 105 (2002) 1534–1536.

[26] R. Hamanaka, G. Mutlu, Particulate Matter Air Pollution: Effects on the Cardiovascular System, Front Endocrinol. (Lausanne) 9 (2018) 680.

[27] J. Wang, Y. Fan, Y. Gao, Q. Hu, T. Wang, TiO_2 nanoparticulatestranslocation and potential toxicological effect in rats after intraarticular injection, Biomaterials 30 (2009) 4590-4600.

[28] J. Lipka, M. Semmler, R. Sperling, A. Wenk, S. Takenaka, C. Schleh, T. Kissel, W. Parak, W. Kreyling, Biodistribution of PEG-modified gold nanoparticulatesfollowing intratracheal instillation and intravenous injection, Biomaterials 31 (2010) 6574–6581.

[29] M. Husain, D. Wu, A. Saber, N. Decan, N. Jacobsen, A. Williams, C. Yauk, H. Wallin, U. Vogel, S. Halappanavar, Intratracheally instilled titanium dioxide nanoparticulatestranslocate to heart and liver and activate complement cascade in the heart of C57BL/6 mice, Nanotoxic. 9 (2015) 1013–1022.

[30] J. Modrzynska, A. Mortensen, T. Berthing, G. Haren, J. Szarek, A. Saber, U. Vogel, Effect on Mouse Liver Morphology of CeO_2, TiO_2 and Carbon Black NanoparticulatesTranslocated from Lungs or Deposited Intravenously, *Appl. Nano* 2 (2021) 222-241.

[31] M. Abdelhalim, B. Jarrar, Gold nanoparticulatesadministration induced prominent inflammatory, central vein intima disruption, fatty change and Kupffer cells hyperplasia, Lipids Health Dis. 10 (2011) 133.

[32] M. Abdelhalim, B. Jarrar, Gold nanoparticulatesinduced cloudy swelling to hydropic degeneration, cytoplasmic hyaline vacuolation, polymorphism, binucleation, karyopyknosis, karyolysis, karyorrhexis and necrosis in the liver, Lipids Health Dis. 10 (2011) 166.

[33] M. Abdelhalim, Gold nanoparticulatesadministration induces disarray of heart muscle, hemorrhagic, chronic inflammatory cells infiltrated by small lymphocytes, cytoplasmic vacuolization and congested and dilated blood vessels, Lipids Health Dis. 10 (2011) 233.

[34] K. Ibrahim, M. Al-Mutary, A. Bakhiet, H. Khan, Histopathology of the Liver, Kidney, and Spleen of Mice Exposed to Gold Nanoparticles, Molecules 23 (2018) 1848.

[35] G. Yan, Y. Huang, Q. Bu, L. Lv, P. Deng, J. Zhou, Y. Wang, Y. Yang, Q. Liu, X. Cen, Y. Zhao, Zinc oxide nanoparticulatescause nephrotoxicity and kidney metabolism alterations in rats. *J. Environ. Sci. Health A Tox. Hazard Subst,* Environ. Eng. 47 (2012) 577-588.

[36] A. Noori, F. Karimi, S. Fatahian, F. Yazdani, Efect of zinc oxide nanoparticulateson renal function in mice, Int. J. Biosc. 5 (2014) 140–146.

[37] M. Behnke, S. Takenaka, S. Fertsch, A. Wenk, J. Seitz, P. Mayer, G. Oberdörster, W. Kreyling, Efficient elimination of inhaled nanoparticulatesfrom the alveolar region: evidence for interstitial uptake and subsequent reentrainment onto airways epithelium, Environ. Health Perspect. 115 (2007) 728–733.

[38] M. Geiser, W. Kreyling, Deposition and biokenetics of inhaled nanoparticles, Part. Fibre Toxicol. 7 (2010) 2–19.

[39] M. Heringa, R. Peters, R. Bleys, M. Lee, P. Tromp, P. Kesteren, J. Eijkeren, A. Undas, A. Oomen, H. Bouwmeester, Detection of titanium particles in human liver and spleen and possible health implications, Part. Fibre Toxicol. 15 (2018) 1–9.

[40] R. Peters, A. Oomen, G. Bemmel, L. Vliet, A. Undas, S. Munniks, R. Bleys, P. Tromp, W. Brand, M. Lee, Silicon dioxide and titanium dioxide particles found in human tissues, Nanotoxic. 14 (2020) 420–432.

[41] Z. Xia, J. Triffitt, A review on macrophage responses to biomaterials, Biomed. Mater. 1 (2006) R1-9.

[42] Z. Sheikh, P. Brooks, O. Barzilay, N. Fine, M. Glogauer, Macrophages, Foreign Body Giant Cells and Their Response to Implantable Biomaterials, Materials (Basel) 2015, 8, 5671-5701.

[43] A. Sergijenko, A. Roelofs, A. Riemen, C. Bari, Bone Marrow Contribution to Synovial Hyperplasia Following Joint Surface Injury, Arthritis Res. Ther. 18 (2016) 166.

[44] M. Amin, D. Fox, J. Ruth, Synovial Cellular and Molecular Markers in Rheumatoid Arthritis, Semin Immunopathol. 39 (2017) 385-393.

[45] C. Burke C, H. Alizai, L. Beltran, R. Regatte, MRI of Synovitis and Joint Fluid, J. Magn. Reson. Imag. 49 (2019) 1512-1527.

[46] J. Allen, C. Manthey, A. Hand, K. Ohura, L. Ellingsworth, S. Wahl, Rapid onset synovial inflammation and hyperplasia induced by transforming growth factor beta, J. Exp. Med. 171 (1990) 231-247.

[47] D. Baeten, E. Kruithof, R. Rycke, A. Boots, H. Mielants, E. Veys, F. Keyser, Infiltration of the synovial membrane with macrophage subsets and polymorphonuclear cells reflects global disease activity in spondyloarthropathy, Arthritis Res. Ther. 7 (2005) R359.

[48] L. Zhang, E. Haddouti, K. Welle, C. Burger, D. Wirtz, F. Schildberg, K. Kabir, The Effects of Biomaterial Implant Wear Debris on Osteoblasts, Front. Cell Develop. Biol. 8 (2020) 352.

[49] D. Pioletti, A. Kottelat, The influence of wear particles in the expression of osteoclastogenesis factors by osteoblasts, Biomaterials 25 (2004) 5803–5808.

[50] S. Goodman, T. Ma, Cellular chemotaxis induced by wear particles from joint replacements, Biomaterials 31 (2010) 5045–5050.

[51] Y. Jiang, T. Jia, P. Wooley, S. Yang, Current research in the pathogenesis of aseptic implant loosening associated with particulate wear debris, Acta. Orthop. Belg. 79 (2013) 1-9.

[52] A. Drynda, S. Drynda, J. Kekow, C. Lohmann, J. Bertrand, Differential effect of cobalt and chromium ions as well as CoCr particles on the expression of osteogenic markers and osteoblast function, Int. J. Mol. Sci. 19 (2018) 3034.

[53] R. Christiansen, H. Münch, C. Bonefeld, J. Thyssen, J. Sloth, C. Geisler, K. Soballe, M. Jallesen, S. Jakobsen, Cytokine profile in patients with aseptic loosening of total hip replacements and its relation to metal release and metal allergy, J. Clin. Med. 8 (2019) 1259.

[54] Z. Wang, Z. Deng, J. Gan, G. Zhou, T. Shi, Z. Wang, Z. Huang, H. Qian, N. Bao, T. Guo, J. Chen, J. Zhang, F. Liu, L. Dong, J. Zhao, TiAl6V4 particles promote osteoclast formation via autophagy-mediated downregulation of interferon-beta in osteocytes, Acta Biomat. 48 (2017) 489-498.

[55] M. Tamai, K. Isama, R. Nakaoka, T. Tsuchiya, Synthesis of a novel b-tricalcium phosphate/hydroxyapatite biphasic calcium phosphate containing niobium ions and evaluation of its osteogenic properties, J. Artif. Organs 10 (2007) 22–28.

[56] A. Obata, Y. Takahashi, T. Miyajima, K. Ueda, T. Narushima, T. Kasuga, Effects of niobium ions released from calcium phosphate invert glasses containing Nb_2O_5 on osteoblast-like cell functions, ACS Appl. Mat. Interf. 4 (2012) 5684-5690.

[57] J. Markhoff, M. Weinmann, C. Schulze, R. Bader, Influence of different grained powders and pellets made of Niobium and Ti-42Nb on human cell viability, Mater. Sc. Eng. C 73 (2017) 756-766.

[58] J. Ge, F. Wang, Z. Xu, X. Shen, C. Gao, D. Wang, G. Hu, J. Gu, T. Tang, J. Wei, Influences of niobium pentoxide on roughness, hydrophilicity, surface energy and protein absorption, and cellular responses to PEEK based composites for orthopedic applications, J. Mat. Chem. B 8 (2020) 2618-2626.

[59] N. Marins, R. Silva, C. Ferrua, D. Łukowiec, A. Barbosa, J. Ribeiro, F. Nedel, E. Zavareze, T. Tański, N. Carreño, Fabrication of electrospun poly(lactic acid) nanoporous membrane loaded with niobium pentoxide nanoparticulatesas a potential scaffold for biomaterial applications, J. Biomed. Mater. Res. Part B: Appl. Biomat. 108 (2020) 1559-1567.

[60] J. Lopes, L. Souza, J. Domingues, F. Ferreira, M. Hausen, J. Camilli, R. Martin, E. Duek, I. Mazali, C. Bertran, *In vitro* and *in vivo* osteogenic potential of niobium-doped 45S5 bioactive glass: A comparative study, J. Biomed. Mater. Res. Part B: Appl. Biomat. 108 (2020) 1372-1387.

[61] L. de Souza, J. Lopes, F. Ferreira, R. Martin, C. Bertran, C. Camilli, Evaluation of effectiveness of 45S5 bioglass doped with niobium for repairing critical-sized bone defect in *in vitro* and *in vivo* models, J. Biomed. Mater. Res. Part A 108 (2020) 446-457.

[62] L. Bonetti, L. Altomare, N. Bono, E. Panno, C. Campiglio, L. Draghi, G. Candiani, S. Farè, A. Boccaccini, L. Nardo, Electrophoretic processing of chitosan based composite scaffolds with Nb-doped bioactive glass for bone tissue regeneration, J. Mat. Science: Mater. Medicine 31 (2020).

[63] M. Niinomi, Fatigue performance and cyto-toxicity of low rigidity titanium alloy, Ti–29Nb–13Ta–4.6Zr, Biomaterials 24 (2003) 2673-2683.

[64] R. Ion, D. Gordin, V. Mitran, P. Osiceanu, S. Dinescu, T. Gloriant, A. Cimpean, *In vitro* bio-functional performances of the novel superelastic beta-type Ti–23Nb–0.7Ta–2Zr–0.5N alloy, Mater. Sc. Eng. C 35 (2014) 411-419.

[65] Y. Zhang, D. Sun, J. Cheng, J. Tsoi, J. Chen, Mechanical and biological properties of Ti–(0–25 wt%)Nb alloys for biomedical implants application, Regen. Biomat. 7 (2020) 119–127.

[66] K. Margevicius, T. Bauer, J. McMahon, S. Brown, K. Merritt, Isolation and characterization of debris in membranes around total joint prostheses, J. Bone Jt. Surg. Am. 76 (1994) 1664-1675.

[67] I. Catelas, O. Huk, A. Petit, D. Zukor, R. Marchand, L. Yahia, Flow cytometric analysis of macrophage response to ceramic and polyethylene particles: effects of size, concentration, and composition, J. Biomed. Mater. Res. 41 (1998) 600-607.

[68] M. Wirth, C. Agrawal, J. Mabrey, D. Dean, C. Blanchard, M. Miller, C. Rockwood Jr, Isolation and characterization of polyethylene wear debris associated with osteolysis following total shoulder arthroplasty, J. Bone Jt. Surg. Am. 81 (1999) 29-37.

[69] C. Lohmann, Z. Schwartz, G. Köster, U. Jahn, G. Buchhorn, M. MacDougall, D. Casasola, Y. Liu, V. Sylvia, D. Dean, B. Boyan, Phagocytosis of wear debris by osteoblasts affects differentiation and local factor production in a manner dependent on particle composition, Biomaterials 21 (2000) 551-561.

[70] S. Yang, W. Ren, Y. Park, A. Sieving, S. Hsu, S. Nasser, P. Wooley, Diverse cellular and apoptotic responses to variant shapes of UHMWPE particles in a murine model of inflammation, Biomaterials 23 (2002) 3535-3543.

[71] S. Lerouge, O. Huk, L. Yahia, L. Sedel, Characterization of *in vivo* wear debris from ceramic-ceramic total hip arthroplasties, J. Bone Jt. Surg. 79B (1996) 135.

[72] A. Hatton, J. Nevelos, A. Nevelos, R. Banks, J. Fisher, E. Ingham, Alumina–alumina artificial hip joints. Part I: a histological analysis and characterisation of wear debris by laser capture microdissection of tissues retrieved at revision, Biomaterials 23 (2002) 3429-3440.

[73] G. Thrivikraman, G. Madras, B. Basu, *In vitro/In vivo* assessment and mechanisms of toxicity of bioceramic materials and its wear particulates, RSC Adv. 4 (2014) 12763.

[74] T. Yoon, S. Rowe, S. Jung, K. Seon, W. Maloney, Osteolysis in association with a total hip arthroplasty with ceramic bearing surfaces, J. Bone Jt. Surg. 80A (1998) 1459.